molecular pharmaceutics

pubs.acs.org/molecularpharmaceutics

Article

Tumor Targeting of ^{211}At-Labeled Antibody under Sodium Ascorbate Protection against Radiolysis

Hiroki Takashima, Kazunobu Ohnuki, Shino Manabe, Yoshikatsu Koga, Ryo Tsumura, Takahiro Anzai, Yang Wang, Xiaojie Yin, Nozomi Sato, Yudai Shigekawa, Akihiro Nambu, Sachiko Usuda, Hiromitsu Haba, Hirofumi Fujii, and Masahiro Yasunaga*

Cite This: *Mol. Pharmaceutics* 2023, 20, 1156−1167

Read Online

ACCESS | Metrics & More | Article Recommendations | Supporting Information

ABSTRACT: Astatine-211 (^{211}At) is an alpha emitter applicable to radioimmunotherapy (RIT), a cancer treatment that utilizes radioactive antibodies to target tumors. In the preparation of ^{211}At-labeled monoclonal antibodies (^{211}At-mAbs), the possibility of radionuclide-induced antibody denaturation (radiolysis) is of concern. Our previous study showed that this ^{211}At-induced radiochemical reaction disrupts the cellular binding activity of an astatinated mAb, resulting in attenuation of *in vivo* antitumor effects, whereas sodium ascorbate (SA), a free radical scavenger, prevents antibody denaturation, contributing to the maintenance of binding and antitumor activity. However, the influence of antibody denaturation on the pharmacokinetics of ^{211}At-mAbs relating to tumor accumulation, blood circulation time, and distribution to normal organs remains unclear. In this study, we use a radioactive anti-human epidermal growth factor receptor 2 (anti-HER2) mAb to demonstrate that an ^{211}At-induced radiochemical reaction disrupts active targeting via an antigen−antibody interaction, whereas SA helps to maintain targeting. In contrast, there was no difference in blood circulation time as well as distribution to normal organs between the stabilized and denatured immunoconjugates, indicating that antibody denaturation may not affect tumor accumulation via passive targeting based on the enhanced permeability and retention effect. In a high-HER2-expressing xenograft model treated with 1 MBq of ^{211}At-anti-HER2 mAbs, SA-dependent maintenance of active targeting contributed to a significantly better response. In treatment with 0.5 or 0.2 MBq, the stabilized radioactive mAb significantly reduced tumor growth compared to the denatured immunoconjugate. Additionally, through a comparison between a stabilized ^{211}At-anti-HER2 mAb and radioactive nontargeted control mAb, we demonstrate that active targeting significantly enhances tumor accumulation of radioactivity and *in vivo* antitumor effect. In RIT with ^{211}At, active targeting contributes to efficient tumor accumulation of radioactivity, resulting in a potent antitumor effect. SA-dependent protection that successfully maintains tumor targeting will facilitate the clinical application of alpha-RIT.

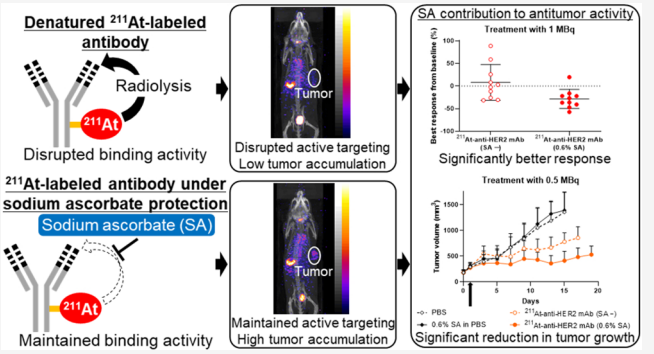

KEYWORDS: *astatine-211, radiolysis, sodium ascorbate, radioactive antibody, tumor targeting, active targeting*

1. INTRODUCTION

Alpha radiation is characterized by a high linear energy transfer at a limited range of 50−100 μm in tissue (equivalent to the thickness of 5−10 cells), compared to other types of ionizing radiation.[1] Therefore, selective accumulation of alpha emitters in tumor tissue results in efficient cancer cell death via deoxyribonucleic acid (DNA) double-strand breaks, without harmful effects on normal cells adjacent to the tumor. Monoclonal antibodies (mAbs) selectively accumulate in tumors via antigen−antibody interaction as well as the enhanced permeability and retention (EPR) effect.[2,3] Tumor targeting via antigen−antibody interaction and the EPR effect is called active targeting and passive targeting, respectively. Therapeutic antibodies such as trastuzumab,[4−8] an anti-human epidermal growth factor receptor 2 (anti-HER2) mAb for breast and gastric cancer, and rituximab,[9−12] an anti-CD20 mAb for non-Hodgkin's lymphoma (NHL) and chronic lymphocytic leukemia (CLL), are clinically available. In addition to naked antibodies, armed antibodies such as antibody−drug conjugates (ADCs) have been clinically approved.[13−15] Antibodies labeled with a therapeutic radionuclide are also considered to be armed antibodies, and cancer

Received: October 18, 2022
Revised: December 1, 2022
Accepted: December 2, 2022
Published: December 27, 2022

treatment that utilizes such radioactive antibodies is called radioimmunotherapy (RIT). Yttrium-90 (^{90}Y) ibritumomab tiuxetan, an anti-CD20 mAb labeled with ^{90}Y, a beta emitter, is indicated for patients with relapsed or refractory low-grade or follicular B-cell NHL and is available for consolidation therapy in patients with follicular NHL who achieve a partial or complete response to first-line chemotherapy.[16−18]

Astatine-211 (^{211}At) is an alpha emitter that has applications in cancer treatment. The radionuclide has the following four favorable properties in this regard. First, its half-life of 7.2 h is long enough to label drug carriers such as antibodies and evaluate antitumor effects and pharmacokinetics.[19] Second, using particle accelerators such as a cyclotron, it is possible to produce a high yield of ^{211}At sufficient to prepare ^{211}At-labeled pharmaceuticals with clinically effective doses of radioactivity.[19] Third, 100% of its decay leads to the production of alpha particles.[19] Fourth, since a daughter nuclide of ^{211}At emits characteristic X-rays, we can image and quantify the biodistribution of ^{211}At-labeled pharmaceuticals by planar scintigraphy and single-photon emission computed tomography (SPECT).[20,21]

Challenges in the preparation process for radionuclide-labeled antibodies include low labeling yield,[22,23] radionuclide release from the antibody,[24−26] and disrupted binding activity[24−28] due to the radionuclide-induced chemical reaction. We previously demonstrated that the ^{211}At-induced radiochemical reaction denatures astatinated mAbs, resulting in disruption of cellular binding and *in vivo* antitumor activity.[29] In addition, we also reported that reactive oxygen species (ROS) generated from the radiolysis of water are able to denature ^{211}At-labeled mAbs (^{211}At-mAbs) and that sodium ascorbate (SA), a free radical scavenger, can successfully quench ROS and protect the immunoconjugate from antibody denaturation in a concentration-dependent manner.[30] These studies revealed that the binding activity of ^{211}At-mAbs stabilized with SA is comparable to that of naked mAb,[29,30] and astatinated mAbs under SA protection exert a significantly greater *in vivo* antitumor effect than the denatured immunoconjugate.[29] However, several questions remain regarding ^{211}At-induced antibody denaturation and SA protection. First, it is not clear whether ^{211}At-induced antibody denaturation has any influence on the blood circulation time of radioactive mAbs. Since longer residence time in the blood results in higher tumor accumulation via passive targeting, this pharmacokinetic parameter is important. Second, whether binding activity disrupted by ^{211}At-induced antibody denaturation affects active targeting of immunoconjugates is unknown. Third, the protective effects of SA on tumor accumulation of ^{211}At-mAbs via passive targeting and active targeting have not been clarified.

In this study, we compared tumor accumulation, residence time in the blood, and distribution to normal organs after administration of ^{211}At-labeled anti-HER2 mAb (^{211}At-anti-HER2 mAb) stabilized with SA and administration of the denatured immunoconjugate in a xenograft model with high HER2 expression. Along with the pharmacokinetic study, we investigated the *in vivo* antitumor effects of denatured and stabilized radioactive mAbs in detail, and gained a deeper understanding of the protective effect of SA on antitumor activity of ^{211}At-mAbs. Additionally, in order to confirm the antitumor mechanism via active targeting, we compared the antitumor effect and tumor accumulation of ^{211}At-anti-HER2 mAb under SA protection with those of a radioactive nontargeted control mAb in a high-HER2-expressing xenograft model.

2. MATERIALS AND METHODS

2.1. Antibodies. Trastuzumab (anti-HER2 mAb) and rituximab (anti-CD20 mAb) were purchased from Chugai Pharmaceutical (Tokyo, Japan) and Nippon Zenyaku Kogyo (Tokyo, Japan), respectively.

2.2. Gastric Cancer Cell Lines and Animal Models. Human gastroesophageal junction cancer cell line OE19 and human gastric cancer cell line NUGC-3 were purchased from the European Collection of Authenticated Cell Cultures (ECACC; London, UK) and the Japanese Collection of Research Bioresources (JCRB; Osaka, Japan), respectively. Human gastric cancer cell line SH-10-TC was purchased from the RIKEN Bioresource Research Center (RIKEN BRC; Tsukuba, Japan). The cells were cultured in RPMI-1640 medium (FUJIFILM Wako Pure Chemical Corporation, Osaka, Japan) supplemented with 10% fetal bovine serum (Thermo Fisher Scientific, Waltham, MA, USA), 100 units/mL penicillin, 100 μg/mL streptomycin, and 0.25 μg/mL amphotericin B (FUJIFILM Wako Pure Chemical Corporation) at 37 °C in a humidified 5% CO_2 atmosphere.

In order to prepare mice bearing subcutaneous tumors, a total of 3×10^6 OE19 cells suspended in 100 μL of phosphate-buffered saline (PBS) were inoculated into the flank regions of five- to six-week-old female BALB/c nu/nu mice (Charles River Japan, Yokohama, Japan). Tumor volume was calculated using the following formula: tumor volume = (length × width^2) × 1/2. Animal experiments were approved by the Committee for Animal Experimentation of the National Cancer Center, Japan. All animal procedures were performed in compliance with the Guidelines for the Care and Use of Experimental Animals established by the Committee. These guidelines meet the ethical standards required by law and comply with the guidelines for the use of experimental animals in Japan.

2.3. HER2 and CD20 Expression. According to a flow cytometry protocol described previously, we evaluated both the expression and number of molecules of HER2 and CD20 in gastric cancer cell lines.[31]

HER2 expression in OE19 subcutaneous tumors was immunohistochemically evaluated as described previously.[31]

2.4. ^{211}At production. ^{211}At was produced with the ^{209}Bi(α,2n)^{211}At reaction using the RIKEN AVF cyclotron (RIKEN, Wako, Japan), and solid ^{211}At was obtained as described previously.[29]

2.5. Preparation of ^{211}At-mAbs. *N*-[2-(maleimido)-ethyl]-3-(trimethylstannyl)benzamide was prepared in two steps using a $PdCl_2(PPh_3)_2$-catalyzed reaction.[32]

Trimethylstannyl-conjugated mAbs (Sn-mAbs) were prepared according to the previously described procedure with minor modifications.[29] In brief, to cleave the disulfide bonds, anti-HER2 mAb and anti-CD20 mAb were reduced at 37 °C for 30 min using 17 and 20 mM cysteamine hydrochloride (Sigma-Aldrich, St. Louis, MO, USA), respectively, and incubated in a 5-fold molar excess of *N*-[2-(maleimido)-ethyl]-3-(trimethylstannyl)benzamide over reactive sulfhydryl groups of each reduced mAb at 4 °C overnight. Then, unconjugated *N*-[2-(maleimido)ethyl]-3-(trimethylstannyl)-benzamides were removed and the buffer solutions were exchanged for PBS through a Vivaspin Turbo Ultrafiltration Unit with a molecular weight cutoff of 30 K (Sartorius,

https://doi.org/10.1021/acs.molpharmaceut.2c00869
Mol. Pharmaceutics 2023, 20, 1156−1167

Göttingen, Germany). Following the previously described procedure, the number of trimethylstannyls per antibody was determined.[29]

We labeled Sn-mAbs with ^{211}At, as previously described.[29] In this study, 93−100 MBq of ^{211}At was added to a Sn-mAb solution. The radioactive mAbs were purified from unlabeled radionuclides and eluted in PBS with or without 0.6% SA (FUJIFILM Wako Pure Chemical Corporation) by size-exclusion chromatography on a PD-10 column (GE Healthcare, Chicago, IL, USA). Radioactivity was measured using a germanium semiconductor detector (GEM P-type or GMX N-type; ORTEC, Zoetermeer, Netherlands) at RIKEN or a curiemeter (IGC-8; HITACHI, Tokyo, Japan) at the National Cancer Center.

2.6. Radiochemical Yield and Radiochemical Purity. Radiochemical yield was calculated by dividing the radioactivity of ^{211}At-mAb fractions collected in a purification process by the initially applied radioactivity. The radiochemical purity of ^{211}At-mAbs was determined by ultrafiltration analysis[29] and validated by protein precipitation with methanol as previously described.[33] Serially, radionuclide release from astatinated mAbs was evaluated at 6, 11, 25, and 50 h after ^{211}At-labeling.

2.7. Sodium Dodecyl Sulfate-Polyacrylamide Gel Electrophoresis (SDS-PAGE). Using a previously established protocol, we performed SDS-PAGE analysis the day after ^{211}At-labeling, and radioactivity and antibodies in the gel were detected.[29]

2.8. Binding Activity. According to a previously described flow cytometry protocol, cellular binding activity of Sn-mAbs and ^{211}At-mAbs was evaluated 6 days after ^{211}At-labeling.[29]

Using a previously described *in vitro* binding assay with minor modifications,[3] we evaluated the binding activity of ^{211}At-mAbs the day after labeling. In brief, serially diluted OE19 or NUGC-3 cells in PBS containing 0.1% bovine serum albumin (BSA) and 2 mM ethylenediaminetetraacetic acid (EDTA) (BE-PBS) were incubated for 30 min on ice with 5 kBq of ^{211}At-mAbs. Then, samples were washed three times with BE-PBS. The radioactivity bound to the cells was counted using a gamma counter (2480 Wizard^2; PerkinElmer, Waltham, MA, USA), and the percentage of cellular binding was calculated by dividing the radioactivity bound to the cells by the initially added radioactivity. The immunoreactivity of ^{211}At-mAbs was determined according to the method of Lindmo et al.[34]

2.9. Cytocidal Effect. As previously described, the *in vitro* cytotoxicity of free ^{211}At diluted in PBS, radionuclide in PBS containing 0.6% SA, ^{211}At-mAbs eluted in PBS, or immunoconjugates in PBS containing 0.6% SA, against OE19, NUGC-3, and SH-10-TC cells was determined using Cell Counting Kit-8 (Dojindo, Kumamoto, Japan).[29]

2.10. SPECT/CT. Model mice bearing OE19 subcutaneous tumors were intravenously administered 1 MBq of ^{211}At-anti-HER2 mAb eluted in PBS, ^{211}At-anti-HER2 mAb eluted in PBS containing 0.6% SA, or ^{211}At-labeled anti-CD20 mAb (^{211}At-anti-CD20 mAb) eluted in PBS containing 0.6% SA. At 1 h after administration, the mice were anesthetized with isoflurane and imaged using a small animal SPECT/CT scanner (NanoSPECT/CT; Mediso, Budapest, Hungary). In order to measure 77−92 keV characteristic X-rays emitted during ^{211}At disintegration,[20] the energy window was set at 83 keV ± 10%. Additionally, SPECT and CT data were sequentially acquired 7 and 19 h after administration of ^{211}At-anti-HER2 mAb eluted in 0.6% SA.

2.11. *Ex Vivo* Biodistribution. OE19 xenograft model mice were randomly divided into three groups and intravenously administered 1 MBq of ^{211}At-anti-HER2 mAb eluted in PBS, ^{211}At-anti-HER2 mAb eluted in PBS containing 0.6% SA, or ^{211}At-anti-CD20 mAb eluted in PBS containing 0.6% SA. At 1, 3.5, 7, and 18 h after administration, blood was collected from the mice under anesthesia with isoflurane. Subsequently, the mice were euthanized and subcutaneous tumors and normal organs were excised. The thyroid gland was collected along with the surrounding subcutaneous tissue, and gastrointestinal contents were washed away with saline. The weight and radioactivity of the biospecimens were measured, and the percentage of injected dose per gram of tissue (%ID/g) was calculated. Radioactivity measurements were conducted using a gamma counter (PerkinElmer).

2.12. *In Vivo* Antitumor Effect. *2.12.1. Experiment 1.* When the tumor volume of OE19 subcutaneous tumors reached approximately 230 mm^3, model mice were randomly divided into four groups and intravenously administered PBS, PBS containing 0.6% SA, 1 MBq of ^{211}At-anti-HER2 mAb eluted in PBS, or 1 MBq of ^{211}At-anti-HER2 mAb eluted in PBS containing 0.6% SA. Tumor volume and body weight were measured once every 2 days. The best response was calculated using the following formula: best response = $(TV_{minimum} - TV_{initial})/TV_{initial} \times 100$, where $TV_{minimum}$ is the minimum tumor volume 7 or more days after administration and $TV_{initial}$ is initial tumor volume.

2.12.2. Experiment 2. When the tumor volume of OE19 subcutaneous tumors reached approximately 180 mm^3, model mice were randomly divided into six groups and intravenously administered PBS, PBS containing 0.6% SA, 0.2 MBq of ^{211}At-anti-HER2 mAb eluted in PBS, 0.2 MBq of ^{211}At-anti-HER2 mAb eluted in PBS containing 0.6% SA, 0.5 MBq of ^{211}At-anti-HER2 mAb in PBS, or 0.5 MBq of ^{211}At-anti-HER2 mAb in 0.6% SA. Tumor volume and body weight were measured once every 2 days.

2.12.3. Experiment 3. When the tumor volume of OE19 subcutaneous tumors reached approximately 230 mm^3, model mice were randomly divided into three groups and intravenously administered PBS containing 0.6% SA, 1 MBq of ^{211}At-anti-HER2 mAb eluted in 0.6% SA, or 1 MBq of ^{211}At-anti-CD20 mAb eluted in 0.6% SA. Tumor volume and body weight were measured once every 2 days.

2.13. Statistical Analysis. *Ex vivo* biodistribution data that did not follow normal distribution (obtained from the lungs 1 h after administration, the small intestine 3.5 h after administration, the stomach and thyroid 7 h after administration, and the heart 18 h after administration) were analyzed using the Kruskal−Wallis test. For *ex vivo* biodistribution data from other biospecimens that did follow normal distribution, one-way ANOVA followed by the Tukey posthoc test was used for analysis. Repeated-measures ANOVA followed by the Tukey posthoc test was used to analyze tumor volume and body weight after treatment. Student's *t* test was used to analyze the differences in the best response between the groups treated with 1 MBq of ^{211}At-anti-HER2 mAb eluted in PBS and 1 MBq of ^{211}At-anti-HER2 mAb eluted in PBS containing 0.6% SA. Statistical analyzes were carried out with SPSS Statistics Version 18 (SPSS, Chicago, IL, USA), and $P < 0.05$ was considered statistically significant.

https://doi.org/10.1021/acs.molpharmaceut.2c00869
Mol. Pharmaceutics 2023, 20, 1156−1167

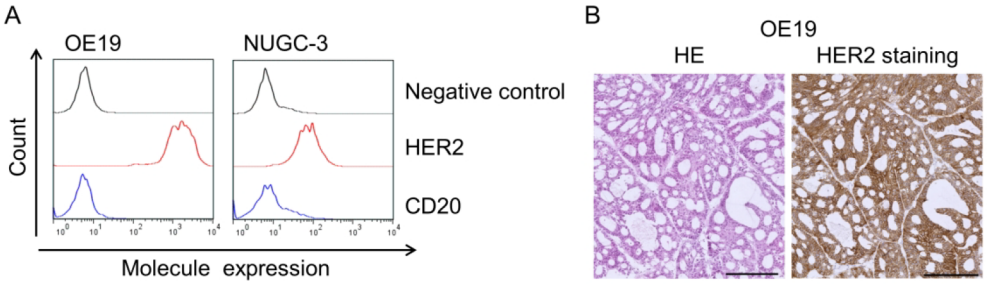

Figure 1. HER2 and CD20 expression on gastric cancer cell lines. (A) Flow cytometry analysis. The numbers of HER2 molecules on OE19 and NUGC-3 cells were 1,245,416 and 86,369 molecules per cell, respectively. CD20 expression on all of these cell lines was negligible. (B) Hematoxylin and eosin (HE) staining and HER2 immunohistochemical analysis. In OE19 subcutaneous tumors, the cancer cells homogeneously expressed HER2. Scale bars, 200 μm.

Table 1. Activity Yields, Radiochemical Yields, and Radiochemical Purities of Astatine-211-Labeled Monoclonal Antibodies (^{211}At-mAbs)[a]

				radiochemical purity (%)	
antibody	sodium ascorbate	activity yield (MBq)	radiochemical yield (%)	ultrafiltration	protein precipitation
trastuzumab	−	33.5 ± 6.1	37.5 ± 7.2	96	96
trastuzumab	+	34.3 ± 4.2	38.0 ± 4.0	98	100
rituximab	−	29.9 ± 11.0	33.2 ± 12.4	95	95
rituximab	+	32.7 ± 9.0	35.9 ± 10.7	95	93

[a]Number of experiments: ^{211}At-anti-HER2 mAb eluted in PBS, n = 7; ^{211}At-anti-HER2 mAb in PBS containing 0.6% sodium ascorbate (SA), n = 8; ^{211}At-anti-CD20 mAb in PBS, n = 5; ^{211}At-anti-CD20 mAb in 0.6% SA, n = 8. Activity yield and radiochemical yield are shown as means ± standard deviation.

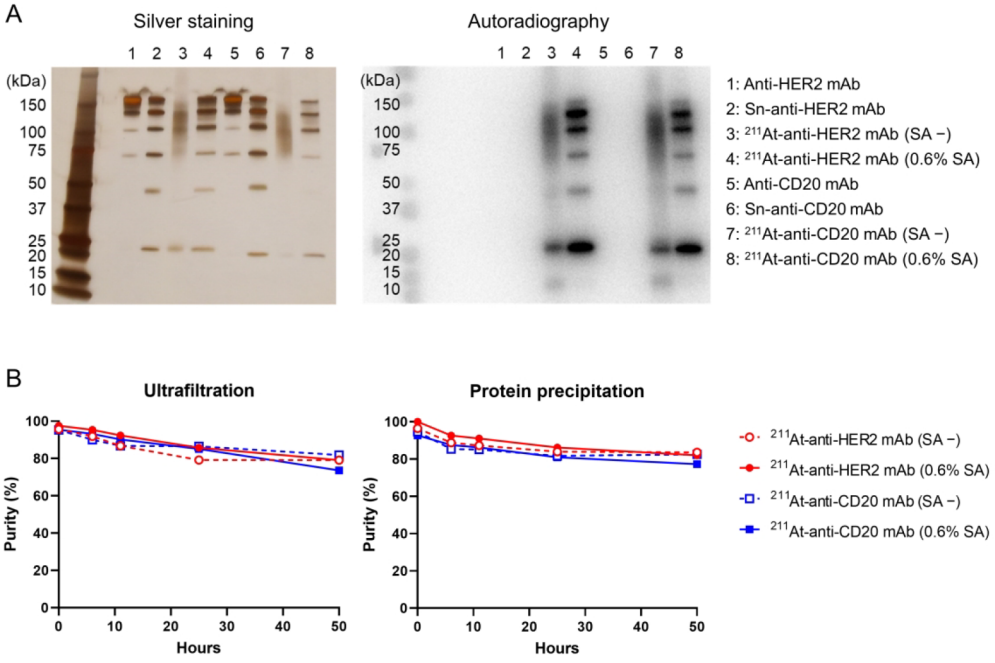

Figure 2. Protective effect of sodium ascorbate (SA) against astatine-211 (^{211}At)-induced antibody denaturation and ^{211}At release from astatinated mAbs. (A) SDS-PAGE analysis. ^{211}At-mAbs eluted in PBS produced smears, whereas ^{211}At-mAbs in PBS containing 0.6% SA yielded band patterns representing trimethylstannyl-conjugated mAbs (Sn-mAbs) and naked mAbs. (B) ^{211}At release from the astatinated mAbs. ^{211}At liberation in PBS was comparable to that in PBS containing 0.6% SA.

3. RESULTS

3.1. HER2 and CD20 Expression. The numbers of HER2 molecules determined by flow cytometry on OE19, NUGC-3, and SH-10-TC cells were 1,245,416, 86,369, and 65,975 molecules per cell, respectively (Figures 1A and S1A). In this study, we defined OE19 as a cell line with high HER2 expression, and NUGC-3 and SH-10-TC as cell lines with low HER2 expression. These cell lines had negligible CD20 expression (Figures 1A and S1A). In OE19 subcutaneous tumors, the cancer cells homogeneously expressed HER2 (Figure 1B).

3.2. ^{211}At-mAbs. The numbers of trimethylstannyl per anti-HER2 mAb and anti-CD20 mAb were 2.44 and 2.52,

https://doi.org/10.1021/acs.molpharmaceut.2c00869
Mol. Pharmaceutics 2023, 20, 1156−1167

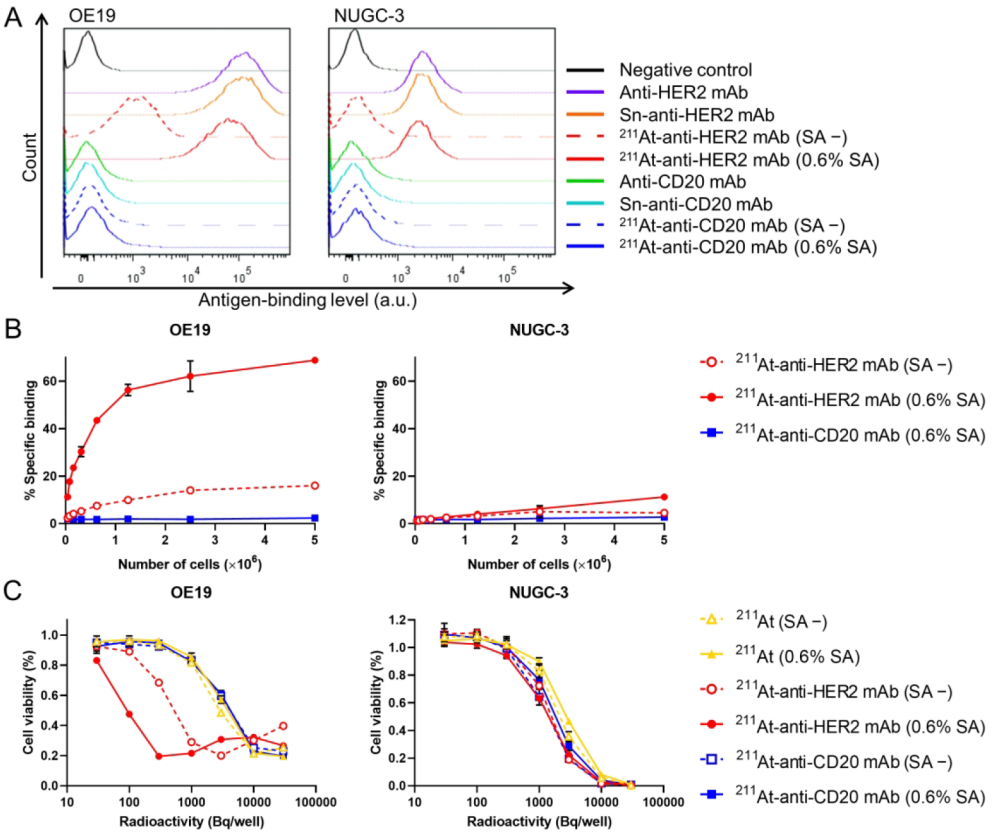

Figure 3. SA protection on binding and cytocidal activity of ^{211}At-mAbs. (A) Flow cytometry analysis. The ^{211}At-induced radiochemical reaction disrupted binding activity of radioactive anti-HER2 mAb eluted in PBS. In contrast, binding activity of ^{211}At-anti-HER2 mAb in PBS containing 0.6% SA was maintained. (B) Immunoreactivity of ^{211}At-mAbs. The immunoreactive fractions of ^{211}At-anti-HER2 mAb eluted in PBS and ^{211}At-anti-HER2 mAb eluted in PBS containing 0.6% SA to OE19 cells were 17% and 75%, respectively. (C) Cytocidal effect. The cytocidal effect of ^{211}At-anti-HER2 mAb eluted in PBS containing 0.6% SA against high-HER2-expressing OE19 cells was greater than astatinated anti-HER2 mAb in PBS. ^{211}At-anti-HER2 mAb in 0.6% SA more efficiently killed OE19 cells expressing high HER2 than free ^{211}At, whereas the cytotoxic effect of ^{211}At-anti-HER2 mAb in 0.6% SA against NUGC-3 cells expressing low HER2 was comparable to free ^{211}At. n = 4. Points, mean; bars, standard deviation.

respectively. Activity yields, defined as the amount of ^{211}At-mAbs expressed in Bq,[35] of ^{211}At-anti-HER2 mAb eluted in PBS, ^{211}At-anti-HER2 mAb in PBS containing 0.6% SA, ^{211}At-anti-CD20 mAb in PBS, and ^{211}At-anti-CD20 mAb in 0.6% SA were 33.5 ± 6.1 MBq, 34.3 ± 4.2 MBq, 29.9 ± 11.0 MBq, and 32.7 ± 9.0 MBq, respectively (Table 1). Radiochemical yields of ^{211}At-anti-HER2 mAb eluted in PBS, ^{211}At-anti-HER2 mAb in PBS containing 0.6% SA, ^{211}At-anti-CD20 mAb in PBS, and ^{211}At-anti-CD20 mAb in 0.6% SA were 37.5 ± 7.2%, 38.0 ± 4.0%, 33.2 ± 12.4%, and 35.9 ± 10.7%, respectively (Table 1). The numbers of labeling experiments for ^{211}At-anti-HER2 mAb eluted in PBS, ^{211}At-anti-HER2 mAb in 0.6% SA, ^{211}At-anti-CD20 mAb in PBS, and ^{211}At-anti-CD20 mAb in 0.6% SA were 7, 8, 5, and 8, respectively. Radiochemical purities of ^{211}At-anti-HER2 mAb eluted in PBS, ^{211}At-anti-HER2 mAb in 0.6% SA, ^{211}At-anti-CD20 mAb in PBS, and ^{211}At-anti-CD20 mAb in 0.6% SA were 96%, 98%, 95%, and 95%, respectively, as determined by ultrafiltration analysis (Table 1). Protein precipitation analysis-based radiochemical purities of ^{211}At-anti-HER2 mAb in PBS, ^{211}At-anti-HER2 mAb in 0.6% SA, ^{211}At-anti-CD20 mAb in PBS, and ^{211}At-anti-CD20 mAb in 0.6% SA were 96%, 100%, 95%, and 93%, respectively (Table 1).

3.3. ^{211}At-Induced Antibody Denaturation, and Radioprotection by SA. In SDS-PAGE analysis, ^{211}At-mAbs eluted in PBS were smeared (Figure 2A), whereas astatinated mAbs eluted in PBS containing 0.6% SA as well as Sn-mAbs were detected as a band pattern, similar to naked mAbs (Figure 2A). These findings suggest that ^{211}At caused denaturation of radioactive mAbs, and that SA protects the immunoconjugates from denaturation.

3.4. ^{211}At Release from Radioactive mAbs. Gradual release of ^{211}At from the immunoconjugates was observed. There was no obvious difference in radionuclide release between ^{211}At-anti-HER2 mAb in PBS, ^{211}At-anti-HER2 mAb in PBS containing 0.6% SA, ^{211}At-anti-CD20 mAb in PBS, and ^{211}At-anti-CD20 mAb in PBS containing 0.6% SA (Figure 2B).

3.5. Cellular Binding Activity. The cellular binding activity of ^{211}At-anti-HER2 mAb eluted in PBS was disrupted compared to naked mAb and Sn-anti-HER2 mAb (Figures 3A and S1B). In contrast, binding of ^{211}At-anti-HER2 mAb stabilized by 0.6% SA was comparable to naked mAb and Sn-anti-HER2 mAb (Figures 3A and S1B). The immunoreactive fraction of ^{211}At-anti-HER2 mAb eluted in PBS and ^{211}At-anti-HER2 mAb eluted in PBS containing 0.6% SA to OE19 cells was 17% and 75%, respectively (Figure 3B). Almost no binding of anti-CD20 mAb, Sn-anti-CD20 mAb, ^{211}At-anti-CD20 mAb eluted in PBS, and ^{211}At-anti-CD20 mAb eluted in 0.6% SA was seen on OE19, NUGC-3, and SH-10-TC gastric cancer cells (Figures 3A,B and S1B).

https://doi.org/10.1021/acs.molpharmaceut.2c00869
Mol. Pharmaceutics 2023, 20, 1156−1167

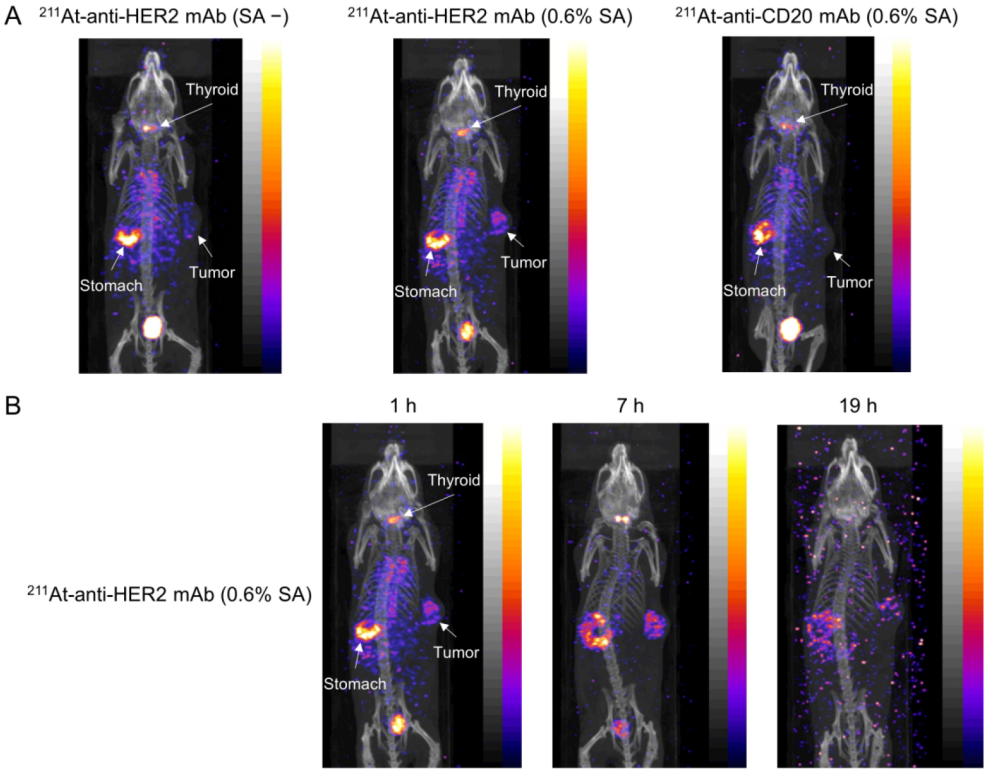

Figure 4. SPECT/CT. (A) OE19 tumor with high HER2 and negligible CD20 expression was more clearly visualized 1 h after administration of ^{211}At-anti-HER2 mAb eluted in PBS containing 0.6% SA compared to ^{211}At-anti-HER2 mAb in PBS or ^{211}At-anti-CD20 mAb in 0.6% SA. In addition to radioactivity uptake in tumors, uptake in the thyroid and stomach was also observed. (B) Sequential images after administration of ^{211}At-anti-HER2 mAb eluted in 0.6% SA.

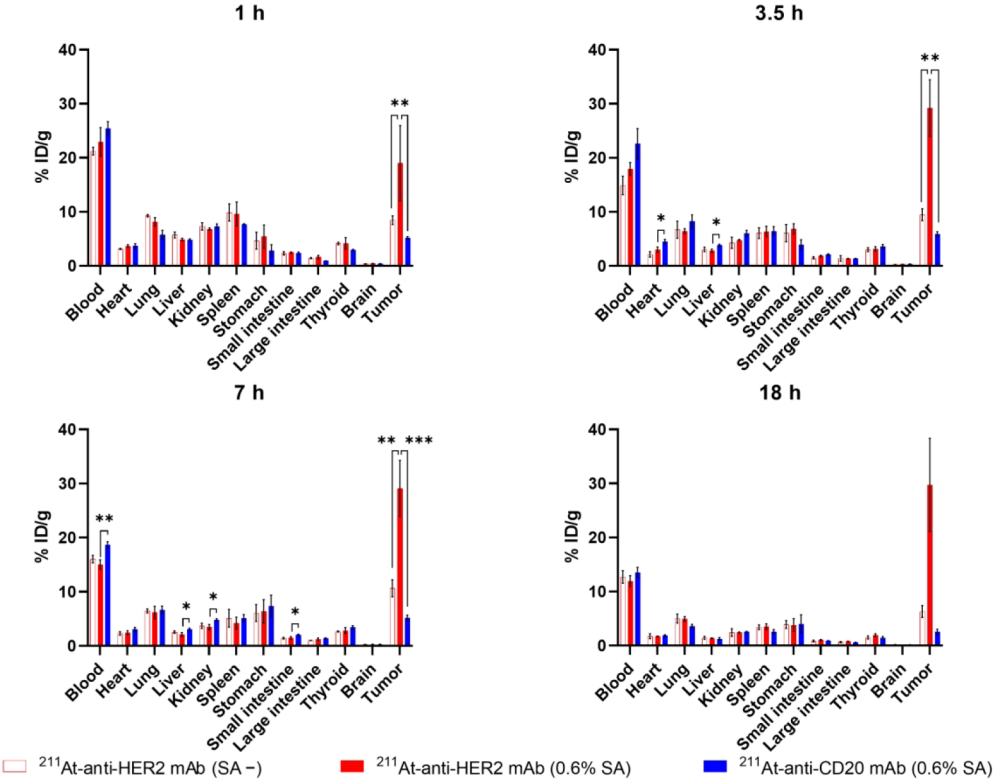

Figure 5. *Ex vivo* biodistribution study. In the OE19 xenograft model with high HER2 and negligible CD20 expression, ^{211}At-anti-HER2 mAb eluted in PBS containing 0.6% SA showed significantly higher tumor accumulation than ^{211}At-anti-HER2 mAb in PBS and ^{211}At-anti-CD20 mAb in 0.6% SA. n = 3. Points, mean; bars, standard deviation. *, $P < 0.05$; **, $P < 0.005$; ***, $P < 0.0005$.

https://doi.org/10.1021/acs.molpharmaceut.2c00869
Mol. Pharmaceutics 2023, 20, 1156−1167

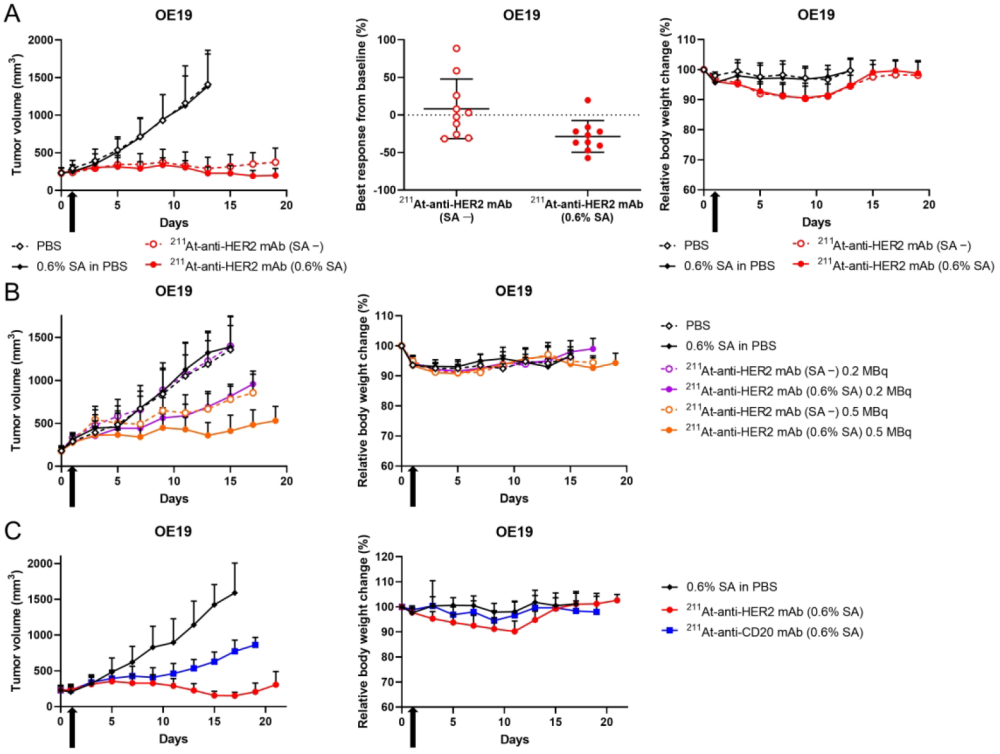

Figure 6. *In vivo* antitumor effect and toxicity. (A) Antitumor effect, best response, and body weight loss in the high-HER2-expressing OE19 xenograft model administered 1 MBq of ^{211}At-anti-HER2 mAb eluted in PBS or 1 MBq of ^{211}At-anti-HER2 mAb in PBS containing 0.6% SA. Arrows, injection; points, mean; bars, standard deviation; number of animals per group, n = 10. (B) Antitumor effect and body weight loss in the high-HER2-expressing OE19 xenograft model administered 0.5 MBq of ^{211}At-anti-HER2 mAb in PBS, 0.5 MBq of ^{211}At-anti-HER2 mAb in 0.6% SA, 0.2 MBq of ^{211}At-anti-HER2 mAb in PBS, or 0.2 MBq of ^{211}At-anti-HER2 mAb in 0.6% SA. Arrows, injection; points, mean; bars, standard deviation; number of animals per group, n = 5. (C) Antitumor effect and body weight loss in the high-HER2- and negligible-CD20-expressing OE19 xenograft model administered 1 MBq of ^{211}At-anti-HER2 mAb in 0.6% SA or 1 MBq of ^{211}At-anti-CD20 mAb in 0.6% SA. Arrows, injection; points, mean; bars, standard deviation; number of animals per group, n = 5.

3.6. Cytocidal Effect. The cytocidal effect of ^{211}At-anti-HER2 mAb eluted in PBS containing 0.6% SA on high-HER2-expressing OE19 cells was greater than astatinated anti-HER2 mAb in PBS (Figure 3C). ^{211}At-anti-HER2 mAb in 0.6% SA more efficiently killed OE19 cells with high expression of HER2 than free ^{211}At, whereas the cytotoxic effect of ^{211}At-anti-HER2 mAb in 0.6% SA on NUGC-3 and SH-10-TC cells with low expression of HER2 was comparable to free ^{211}At (Figures 3C and S1C). The cytotoxicity of ^{211}At-anti-CD20 mAb in 0.6% SA against cancer cells with negligible expression of CD20 was comparable to free ^{211}At (Figures 3C and S1C).

3.7. *In Vivo* SPECT/CT Images. In the high-HER2- and negligible-CD20-expressing OE19 xenograft model, the SPECT/CT signal in the tumor 1 h after administration of ^{211}At-anti-HER2 mAb eluted in PBS containing 0.6% SA was more clearly visualized than after administration of ^{211}At-anti-HER2 mAb eluted in PBS or ^{211}At-anti-CD20 mAb eluted in PBS containing 0.6% SA (Figure 4A). In addition to the tumor, signal accumulation was observed in the thyroid and stomach as well (Figure 4A).

Signal in the tumor, thyroid, and stomach was retained 7 h after administration of ^{211}At-anti-HER2 mAb eluted in 0.6% SA, whereas signal intensity in the blood decreased (Figure 4B).

3.8. *Ex Vivo* Biodistribution. *Ex vivo* biodistribution analysis of the OE19 xenograft model revealed that tumor accumulation of ^{211}At-anti-HER2 mAb eluted in PBS containing 0.6% SA was significantly higher than that of ^{211}At-anti-HER2 mAb eluted in PBS at 1 h (P = 0.043), 3.5 h (P = 0.035), and 7 h (P < 0.001) after administration (Figure 5). On the other hand, there was no difference in %ID/g for the blood and normal organs between the groups administered ^{211}At-anti-HER2 mAb in PBS and ^{211}At-anti-HER2 mAb in 0.6% SA (Figure 5).

^{211}At-anti-HER2 mAb eluted in 0.6% SA showed significantly higher tumor accumulation than ^{211}At-anti-CD20 mAb in 0.6% SA 1 h (P = 0.013), 3.5 h (P = 0.029), and 7 h (P < 0.001) after administration (Figure 5). On the other hand, %ID/g for the heart (P = 0.020) and liver (P = 0.018) 3.5 h after administration of ^{211}At-anti-CD20 mAb in 0.6% SA was significantly higher than that after administration of ^{211}At-anti-HER2 mAb in 0.6% SA (Figure 5). In addition, ^{211}At-anti-CD20 mAb in 0.6% SA was retained in the blood (P = 0.002), liver (P = 0.011), kidney (P = 0.019), and small intestine (P = 0.030) at 7 h postinjection compared to ^{211}At-anti-HER2 mAb in 0.6% SA (Figure 5).

At 7 h after administration of ^{211}At-anti-HER2 mAb eluted in PBS containing 0.6% SA, %ID/g values for the tumor and blood were 29.11 ± 5.18% and 15.03 ± 0.89%, respectively (Figure 5), which was consistent with the SPECT/CT image showing a high contrast signal in the tumor (Figure 4B). In contrast to the SPECT/CT study (Figure 4A), %ID/g values for the stomach and thyroid were lower than that for the blood at 1 h after administration of ^{211}At-anti-HER2 mAb in PBS, ^{211}At-anti-HER2 mAb in 0.6% SA, or ^{211}At-anti-CD20 mAb in 0.6% SA (Figure 5).

https://doi.org/10.1021/acs.molpharmaceut.2c00869
Mol. Pharmaceutics 2023, 20, 1156−1167

3.9. *In Vivo* Antitumor Effect and Toxicity. Although there was no significant difference in OE19 tumor growth between the groups administered 1 MBq of ^{211}At-anti-HER2 mAb eluted in PBS and 1 MBq of ^{211}At-anti-HER2 mAb eluted in PBS containing 0.6% SA, the best response after administration of ^{211}At-anti-HER2 mAb in PBS containing 0.6% SA was significantly better than that of ^{211}At-anti-HER2 mAb in PBS (P = 0.018) (Figure 6A). The best response for treatment with ^{211}At-anti-HER2 mAb in 0.6% SA was −28.58 ± 21.08%, indicating tumor regression from baseline, whereas ^{211}At-anti-HER2 mAb in PBS did not result in tumor regression (the best response was 8.19 ± 39.61% (Figure 6A)). Body weight loss in the group administered 1 MBq of ^{211}At-anti-HER2 mAb in 0.6% SA was transient and comparable to 1 MBq of ^{211}At-anti-HER2 mAb in PBS (Figure 6A).

In the OE19 xenograft model, 0.5 MBq of ^{211}At-anti-HER2 mAb in 0.6% SA induced significantly reduced tumor growth than 0.5 MBq of ^{211}At-anti-HER2 mAb in PBS (P = 0.001) (Figure 6B). When 0.2 MBq of ^{211}At-mAbs was administered, there was no difference in tumor growth between the groups administered PBS, PBS containing 0.6% SA, and ^{211}At-anti-HER2 mAb in PBS. In contrast, ^{211}At-anti-HER2 mAb in 0.6% SA induced significantly greater antitumor effects relative to PBS, PBS containing 0.6% SA, and ^{211}At-anti-HER2 mAb in PBS (PBS vs 0.2 MBq of ^{211}At-anti-HER2 mAb [0.6% SA], P = 0.001; 0.6% SA in PBS vs 0.2 MBq of ^{211}At-anti-HER2 mAb [0.6% SA], P < 0.001; 0.2 MBq of ^{211}At-anti-HER2 mAb [SA −] vs 0.2 MBq of ^{211}At-anti-HER2 mAb [0.6% SA], P < 0.001) (Figure 6B). When 0.2 MBq or 0.5 MBq of ^{211}At-mAbs was administered, significant body weight loss relative to PBS or PBS containing 0.6% SA was not observed (Figure 6B).

In the OE19 xenograft model with high HER2 and negligible CD20 expression, 1 MBq of ^{211}At-anti-HER2 mAb in 0.6% SA exerted significantly greater antitumor effects than 1 MBq of ^{211}At-anti-CD20 mAb in 0.6% SA (P < 0.001) (Figure 6C). Body weight loss after administration of these radioactive immunoconjugates was transient (Figure 6C).

4. DISCUSSION

Larsen et al. reported that adding free ^{211}At into an antibody solution results in disruption of the antigen−antibody interaction in a radioactivity- and dose-dependent manner.[28] From the SDS-PAGE analysis in this study, ^{211}At-anti-HER2 and ^{211}At-anti-CD20 mAbs eluted in PBS containing 0.6% SA yielded band patterns that were similar to Sn-mAbs and naked mAbs, whereas ^{211}At-mAbs eluted in PBS yielded smears rather than discernible bands, suggesting radionuclide-induced antibody denaturation (Figure 2A). Consistently, cellular binding activity of ^{211}At-anti-HER2 mAb in PBS was disrupted, and that of the astatinated anti-HER2 mAb in 0.6% SA was comparable to naked mAb as well as Sn-mAb (Figure 3A). Similarly, using a mAb recognizing tissue factor, we demonstrated that astatinated mAbs eluted in PBS are denatured and that SA successfully protects the immunoconjugate from antibody denaturation.[29] It appears that the ^{211}At-induced radiochemical reaction universally denatures astatinated mAbs regardless of the antibody clone. Focusing on the mechanism of ^{211}At-induced antibody denaturation as well as the mode of action of SA-mediated prevention of denaturation, we revealed that ROS generated via ^{211}At-induced water radiolysis cause denaturation of antibodies, while reducing agents such as SA protect ^{211}At-labeled antibodies by quenching ROS in a concentration-dependent manner.[30] A study conducted to determine the concentration at which SA exerts protective activity found that 0.6% SA completely quenches ROS after radiolabeling with 100 MBq of ^{211}At.[30] Thus, in this study, we used 0.6% SA in order to protect mAbs labeled with ^{211}At. For ^{211}At labeling, we added 93−100 MBq of ^{211}At to Sn-mAb solutions. As a result, the activity yields of ^{211}At-anti-HER2 mAb eluted in PBS, ^{211}At-anti-HER2 mAb in PBS containing 0.6% SA, ^{211}At-anti-CD20 mAb in PBS, and ^{211}At-anti-CD20 mAb in 0.6% SA were 33.5 ± 6.1 MBq, 34.3 ± 4.2 MBq, 29.9 ± 11.0 MBq, and 32.7 ± 9.0 MBq, respectively (Table 1). In clinical studies, ^{211}At-mAbs with higher radioactivity were prepared and administered to patients. In a clinical study of ^{211}At-labeled anti-tenascin mAb, the two-step procedure for ^{211}At labeling yielded 104−518 MBq of radioactive mAbs,[36] and patients with recurrent glioma were treated by injecting 70.7−347.1 MBq of ^{211}At-labeled anti-tenascin mAbs into a surgically created resection cavity.[37] No dose-limiting toxicity was observed, and the maximum tolerated dose was not determined in the study. Recently, a revised two-step procedure was designed, which yields 70.7−1024 MBq of ^{211}At-labeled anti-tenascin mAbs and makes further dose escalation feasible.[38] In a clinical study of ^{211}At-labeled anti-NaPi2b F(ab′)$_2$ fragments, patients with relapsed ovarian cancer received 34−355 MBq of the radioactive F(ab′)$_2$ fragments through intraperitoneal injection.[39] Li et al. reported cGMP production of ^{211}At-labeled anti-CD45 mAb, which yields 800−1280 MBq of the radioactive immunoconjugates.[40] Since higher radioactivity and radiation dose promote ^{211}At-induced antibody denaturation,[28] appropriate caution must be exercised in radiolabeling with highly radioactive ^{211}At for clinical use. In addition to radioactivity, concentration of radiopharmaceuticals[41] and volume of solution containing radioactive mAbs[42] seem to have an effect on radiolysis. Considering these factors, it is important to optimize storage conditions such as concentration of SA.[30] With regard to ^{211}At liberation, ^{211}At was gradually released from both ^{211}At-anti-HER2 mAb and ^{211}At-anti-CD20 mAb (Figure 2B). Carbon−astatine bond strength is relatively weaker than other carbon−halogen bonds.[42,43] That may be one of the reasons why the gradual release was observed in PBS. Additionally, Dekempeneer et al. compared the stability in PBS between the astatinated nanobody site specifically conjugated with *N*-[2-(maleimido)ethyl]-3-(trimethylstannyl)-benzamide via the C-terminal cysteine and the radioactive nanobody conjugated with *N*-succinimidyl-3-(trimethylstannyl)benzoate via the lysine residues. They demonstrated that ^{211}At is gradually released from the astatinated nanobody conjugated with *N*-[2-(maleimido)-ethyl]-3-(trimethylstannyl)benzamide, but not the radioactive nanobody conjugated with *N*-succinimidyl-3-(trimethylstannyl)benzoate.[44] Although our ^{211}At-mAbs differ in terms of the full-length antibody conjugated with *N*-[2-(maleimido)ethyl]-3-(trimethylstannyl)benzamide via the cysteine residues in the hinge region, a thioether bond between the sulfhydryl and maleimide groups may cause ^{211}At release in PBS. On the other hand, Teze et al. reported that hydroxyl radicals promote oxidative dehalogenation of astatobenzoate conjugates.[45] However, ^{211}At-induced antibody denaturation as well as ROS does not appear to cause radionuclide release from both ^{211}At-anti-HER2 mAb and ^{211}At-anti-CD20 mAb

https://doi.org/10.1021/acs.molpharmaceut.2c00869
Mol. Pharmaceutics 2023, 20, 1156−1167

under these experimental conditions, since ^{211}At liberation in PBS containing 0.6% SA was comparable to that in PBS alone (Figure 2B).

^{211}At-anti-HER2 mAb eluted in PBS containing 0.6% SA exerted a greater cytocidal effect against OE19 cells with high expression of HER2 than the immunoconjugate eluted in PBS (Figure 3C). Astatinated mAbs stabilized with SA showed cytotoxicity against gastric cancer cells that was dependent on the level of the target molecule on the cell membrane. ^{211}At-anti-HER2 mAb eluted in 0.6% SA more efficiently killed OE19 cells expressing high HER2 than free ^{211}At, whereas cytotoxicity against NUGC-3 and SH-10-TC cells expressing low HER2 was comparable to free ^{211}At (Figure 3C and S1C). On the other hand, the cytocidal effects of ^{211}At-anti-CD20 mAb in 0.6% SA against OE19, NUGC-3, and SH-10-TC cells with negligible CD20 expression were comparable to those of free ^{211}At (Figure 3C and S1C). This indicates that higher target molecular expression on cancer cells than the threshold is necessary for ^{211}At-anti-mAbs under SA protection to exert greater cytocidal activity relative to free ^{211}At.

The SPECT/CT study demonstrated that OE19 tumors were more clearly visualized after administration of ^{211}At-anti-HER2 mAb eluted in PBS containing 0.6% SA compared to ^{211}At-anti-HER2 mAb in PBS or ^{211}At-anti-CD20 mAb in PBS containing 0.6% SA (Figure 4A). Consistently, the *ex vivo* biodistribution study revealed that tumor accumulation of ^{211}At-anti-HER2 mAb in 0.6% SA was significantly higher than that of ^{211}At-anti-HER2 mAb in PBS and ^{211}At-anti-CD20 mAb in 0.6% SA (Figure 5). As a result of this disrupted binding activity (Figures 3A,B), active targeting of ^{211}At-anti-HER2 mAb eluted in PBS was attenuated, resulting in significantly lower tumor accumulation than astatinated anti-HER2 mAb stabilized with 0.6% SA (Figures 4A and 5). The ^{211}At-induced radiochemical reaction disrupts active targeting of radioactive mAbs, whereas SA successfully maintains tumor targeting. In contrast, ^{211}At-induced antibody denaturation does not seem to affect tumor accumulation via passive targeting based on the EPR effect,[2] since there was no difference in blood circulation time as well as distribution to normal organs between the groups administered ^{211}At-anti-HER2 mAb in PBS and ^{211}At-anti-HER2 mAb in 0.6% SA (Figure 5). Although it was speculated that ^{211}At-induced antibody denaturation might cause a structural change that increases distribution of astatinated anti-HER2 mAb to various organs, %ID/g for normal organs after administration of denatured radioactive mAb was comparable to that after administration of the immunoconjugate stabilized with SA (Figure 5). On the other hand, although %ID for tumor was higher than that for blood at 3.5, 7, and 18 h after administration of ^{211}At-anti-HER2 mAb in 0.6% SA, successful tumor accumulation was not observed after administration of ^{211}At-anti-HER2 mAb in PBS or ^{211}At-anti-CD20 mAb in 0.6% SA (Figure 5). These three immunoconjugates were macroproteins with molecular weights of 150 kDa and met the requirement for tumor accumulation via passive targeting.[2] However, ^{211}At-anti-HER2 mAb in PBS and ^{211}At-anti-CD20 mAb in 0.6% SA failed to show higher accumulation of radioactivity in tumors relative to blood (Figure 5). With regard to active targeting, the binding activity of ^{211}At-anti-HER2 mAb in 0.6% SA with HER2 was intact, whereas that of ^{211}At-anti-HER2 mAb in PBS and ^{211}At-anti-CD20 mAb in 0.6% SA was disrupted and negligible, respectively (Figure 3A,B). ^{211}At-anti-HER2 mAb in 0.6% SA showed higher accumulation in tumors than blood, but ^{211}At-anti-HER2 mAb in PBS as well as ^{211}At-anti-CD20 mAb in 0.6% SA did not (Figure 5). Accordingly, in ^{211}At-RIT, active targeting mainly seems to contribute to selective tumor accumulation of radioactivity.

In addition to radioactivity uptake in tumors, SPECT/CT demonstrated uptake in the stomach and thyroid after administration of ^{211}At-mAbs (Figure 4A,B). Free ^{211}At accumulates in the thyroid and stomach,[21,46−48] which is different from the biodistribution of mAbs labeled with indium-111 (^{111}In) or zirconium-89 (^{89}Zr).[49−51] Therefore, ^{211}At released from these astatinated mAbs appears to cause signal accumulation in the thyroid and stomach. Although the SPECT/CT study revealed that signals in the stomach and thyroid were higher than those in the blood pool at 1 h after administration of ^{211}At-mAbs (Figure 4A), the *ex vivo* biodistribution study demonstrated that %ID/g values for the stomach and thyroid were lower than that for the blood (Figure 5). In this study, we collected thyroid glands along with the surrounding subcutaneous tissue, which resulted in a heavier tissue weight and lower %ID/g. On the other hand, gastrointestinal contents were washed away with saline prior to measuring radioactivity in the stomach. Iodine-131 (^{131}I) is secreted into gastric juice.[52,53] Since astatine, like iodine, belongs to the halogen family, ^{211}At also appears to be secreted into gastric juice. In fact, Liu et al. demonstrated that mice intravenously administered ^{211}At show distribution to the stomach contents as well as the stomach, and both %ID and %ID/g for the stomach contents are higher than those for the stomach.[47] SPECT scanning detected signals not only in the stomach but also in the stomach contents, whereas in the *ex vivo* biodistribution study, free ^{211}At in the stomach contents was washed away prior to measuring radioactivity in the stomach. This may explain the discrepancy with regard to radioactivity uptake in the blood, thyroid, and stomach between the SPECT/CT and *ex vivo* biodistribution studies (Figures 4A and 5). Since SPECT/CT successfully detected thyroid and stomach uptake derived from free ^{211}At, the *in vivo* imaging is useful for evaluating ^{211}At release from the immunoconjugate.

The *ex vivo* biodistribution study demonstrated that %ID/g for the blood collected from mice administered ^{211}At-anti-CD20 mAb eluted in PBS containing 0.6% SA was significantly higher than that collected from mice administered ^{211}At-anti-HER2 mAb in 0.6% SA 7 h postinjection (Figure 5). This finding suggests that ^{211}At-anti-CD20 mAb in 0.6% SA had a longer residence time than ^{211}At-anti-HER2 mAb in 0.6% SA, which might result in a significantly higher %ID/g for normal organs after administration of astatinated anti-CD20 mAb such as in the heart and liver at 3.5 h postinjection, and liver, kidney, and small intestine at 7 h postinjection. In contrast, ^{211}At-anti-HER2 mAb eluted in PBS containing 0.6% SA showed significantly higher tumor accumulation in the OE19 xenograft model compared to ^{211}At-anti-CD20 mAb eluted in 0.6% SA (Figure 5), which suggests that active targeting via antigen−antibody interaction significantly increases tumor accumulation of ^{211}At-mAbs.

There was no significant difference in OE19 tumor growth between the groups administered 1 MBq of ^{211}At-anti-HER2 mAb eluted in PBS and 1 MBq of ^{211}At-anti-HER2 mAb eluted in PBS containing 0.6% SA, whereas the best response after administration of ^{211}At-anti-HER2 mAb in 0.6% SA was

https://doi.org/10.1021/acs.molpharmaceut.2c00869
Mol. Pharmaceutics 2023, 20, 1156−1167

significantly better than ^{211}At-anti-HER2 mAb in PBS (Figure 6A). In summary, in treatments with 1 MBq of ^{211}At-mAbs, stabilization of immunoconjugates with SA contributed to the best response after administration, but did not reduce tumor growth. On the other hand, when lower radioactive doses such as 0.5 or 0.2 MBq were administered, SA stabilization had a more obvious impact on antitumor activity, and ^{211}At-anti-HER2 mAb in 0.6% SA more efficiently reduced OE19 tumor growth than ^{211}At-anti-HER2 mAb in PBS (Figure 6B). Treatment with 0.2 MBq resulted in tumor growth after administration of ^{211}At-anti-HER2 mAb eluted in PBS, which was comparable to that after administration of PBS or PBS containing 0.6% SA. In other words, 0.2 MBq of the denatured immunoconjugate showed no antitumor activity. Contrary to the denatured radioactive mAb, 0.2 MBq of ^{211}At-anti-HER2 mAb stabilized with 0.6% SA exerted significantly greater antitumor effects relative to PBS and PBS containing 0.6% SA (Figure 6B). The tumor-absorbed dose did not reach therapeutic range after administration of 0.2 MBq of ^{211}At-anti-HER2 mAb eluted in PBS due to the disrupted tumor targeting, whereas SA protection maintained tumor targeting (Figures 4A and 5), resulting in a therapeutic absorbed dose in tumors even after administration of low radioactivity. Additionally, the difference in cytocidal effect between the denatured and stabilized ^{211}At-mAbs contributed to *in vivo* antitumor activity (Figures 3C and 6A,B).

In the high-HER2- and negligible-CD20-expressing OE19 xenograft model, ^{211}At-anti-HER2 mAb eluted in PBS containing 0.6% SA exerted a significantly greater antitumor effect than ^{211}At-anti-CD20 mAb eluted in 0.6% SA (Figure 6C). In the *ex vivo* biodistribution study, radioactivity accumulation in OE19 tumors at 1, 3.5, and 7 h after administration of ^{211}At-anti-HER2 mAb in 0.6% SA was significantly higher than that after administration of the radioactive nontargeted control mAb (Figure 5). These results indicate that active targeting contributes to efficient tumor accumulation of radioactivity, resulting in significantly greater antitumor activity.

5. CONCLUSIONS

In ^{211}At-RIT, active targeting significantly enhances tumor accumulation of radioactivity and contributes to a potent antitumor effect. SA-dependent protection that successfully maintains both tumor targeting and cytocidal activity of ^{211}At-mAbs will facilitate the clinical application of the alpha-RIT.

■ ASSOCIATED CONTENT

Supporting Information

The Supporting Information is available free of charge at https://pubs.acs.org/doi/10.1021/acs.molpharmaceut.2c00869.

HER2 and CD20 expression on SH-10-TC cells; cellular binding activity of ^{211}At-anti-HER2 mAb eluted in PBS, ^{211}At-anti-HER2 mAb in PBS containing 0.6% SA, ^{211}At-anti-CD20 mAb in PBS, and ^{211}At-anti-CD20 mAb in 0.6% SA; cytocidal effect of these astatinated mAbs against SH-10-TC cells (PDF)

■ AUTHOR INFORMATION

Corresponding Author

Masahiro Yasunaga − *Division of Developmental Therapeutics, Exploratory Oncology Research & Clinical Trial Center, National Cancer Center, Kashiwa, Chiba 277-8577, Japan;* orcid.org/0000-0003-3356-0197; Phone: +81-4-7134-6857; Email: mayasuna@east.ncc.go.jp; Fax: +81-4-7134-6866

Authors

Hiroki Takashima − *Division of Developmental Therapeutics, Exploratory Oncology Research & Clinical Trial Center, National Cancer Center, Kashiwa, Chiba 277-8577, Japan;* orcid.org/0000-0001-6487-7344

Kazunobu Ohnuki − *Division of Functional Imaging, Exploratory Oncology Research & Clinical Trial Center, National Cancer Center, Kashiwa, Chiba 277-8577, Japan*

Shino Manabe − *Laboratory of Functional Molecule Chemistry, Pharmaceutical Department and Institute of Medicinal Chemistry, Hoshi University, Shinagawa-ku, Tokyo 142-8501, Japan; Research Center for Pharmaceutical Development, Graduate School of Pharmaceutical Sciences & Faculty of Pharmaceutical Sciences, Tohoku University, Aoba-ku, Sendai 980-8578, Japan; Glycometabolic Biochemistry Laboratory, RIKEN, Wako, Saitama 351-0198, Japan;* orcid.org/0000-0002-2763-1414

Yoshikatsu Koga − *Division of Developmental Therapeutics and Department of Strategic Programs, Exploratory Oncology Research & Clinical Trial Center, National Cancer Center, Kashiwa, Chiba 277-8577, Japan*

Ryo Tsumura − *Division of Developmental Therapeutics, Exploratory Oncology Research & Clinical Trial Center, National Cancer Center, Kashiwa, Chiba 277-8577, Japan*

Takahiro Anzai − *Division of Developmental Therapeutics, Exploratory Oncology Research & Clinical Trial Center, National Cancer Center, Kashiwa, Chiba 277-8577, Japan*

Yang Wang − *Nishina Center for Accelerator-Based Science, RIKEN, Wako, Saitama 351-0198, Japan*

Xiaojie Yin − *Nishina Center for Accelerator-Based Science, RIKEN, Wako, Saitama 351-0198, Japan*

Nozomi Sato − *Nishina Center for Accelerator-Based Science, RIKEN, Wako, Saitama 351-0198, Japan*

Yudai Shigekawa − *Nishina Center for Accelerator-Based Science, RIKEN, Wako, Saitama 351-0198, Japan*

Akihiro Nambu − *Nishina Center for Accelerator-Based Science, RIKEN, Wako, Saitama 351-0198, Japan*

Sachiko Usuda − *Nishina Center for Accelerator-Based Science, RIKEN, Wako, Saitama 351-0198, Japan*

Hiromitsu Haba − *Nishina Center for Accelerator-Based Science, RIKEN, Wako, Saitama 351-0198, Japan*

Hirofumi Fujii − *Division of Functional Imaging, Exploratory Oncology Research & Clinical Trial Center, National Cancer Center, Kashiwa, Chiba 277-8577, Japan*

Complete contact information is available at: https://pubs.acs.org/10.1021/acs.molpharmaceut.2c00869

Author Contributions

H.T., S.M., and M.Y. contributed to the study conception and design. H.T. acquired and analyzed the data, and wrote the first draft of the manuscript. S.M. prepared *N*-[2-(maleimido)-ethyl]-3-(trimethylstannyl)benzamide and acquired the data. K.O., Y.K., R.T., and T.A. acquired and analyzed the data. Y.W., X.Y., N.S., Y.S., A.N., S.U., and H.H. contributed to ^{211}At production. H.T., S.M., H.H., H.F., and M.Y. revised the manuscript. All authors read and approved the final manuscript.

Notes

The authors declare no competing financial interest.

■ ACKNOWLEDGMENTS

This work was supported by the Project for Cancer Research and Therapeutic Evolution (19 cm0106237h0002 to H.T.) from the Japan Agency for Medical Research and Development (AMED), the Japan Society for the Promotion of Science (JSPS) Grant-in-Aid for Early-Career Scientists (22K15594 to H.T.), the National Cancer Center Research and Development Fund (30-S-4 to Y.K. and 2020-A-9 to M.Y.), and the RIKEN Engineering Network Project (to S.M.). ^{211}At was supplied through the Supply Platform of Short-lived Radioisotopes, supported by the JSPS Grant-in-Aid for Scientific Research on Innovative Areas (16H06278).

■ ABBREVIATIONS

ADC; antibody−drug conjugate; ^{211}At; astatine-211; BE-PBS; phosphate-buffered saline containing 0.1% bovine serum albumin and 2 mM ethylenediaminetetraacetic acid; ^{209}Bi; bismuth-209; BSA; bovine serum albumin; CLL; chronic lymphocytic leukemia; CT; computed tomography; DNA; deoxyribonucleic acid; EDTA; ethylenediaminetetraacetic acid; EPR effect; enhanced permeability and retention effect; HER2; human epidermal growth factor receptor 2; HE staining; hematoxylin and eosin staining; ^{131}I; iodine-131; ID; injected dose; ^{111}In; indium-111; mAb; monoclonal antibody; NHL; non-Hodgkin's lymphoma; PBS; phosphate-buffered saline; RIT; radioimmunotherapy; ROS; reactive oxygen species; SA; sodium ascorbate; SDS-PAGE; sodium dodecyl sulfate-polyacrylamide gel electrophoresis; SPECT; single-photon emission computed tomography; ^{90}Y; yttrium-90; ^{89}Zr; zirconium-89.

■ REFERENCES

(1) Aghevlian, S.; Boyle, A. J.; Reilly, R. M. Radioimmunotherapy of cancer with high linear energy transfer (LET) radiation delivered by radionuclides emitting α-particles or Auger electrons. *Advanced drug delivery reviews* **2017**, *109*, 102−118.

(2) Matsumura, Y.; Maeda, H. A new concept for macromolecular therapeutics in cancer chemotherapy: mechanism of tumoritropic accumulation of proteins and the antitumor agent smancs. *Cancer Res.* **1986**, *46*, 6387−6392.

(3) Takashima, H.; Tsuji, A. B.; Saga, T.; Yasunaga, M.; Koga, Y.; Kuroda, J. I.; Yano, S.; Kuratsu, J. I.; Matsumura, Y. Molecular imaging using an anti-human tissue factor monoclonal antibody in an orthotopic glioma xenograft model. *Sci. Rep* **2017**, *7* (1), 12341.

(4) Slamon, D. J.; Leyland-Jones, B.; Shak, S.; Fuchs, H.; Paton, V.; Bajamonde, A.; Fleming, T.; Eiermann, W.; Wolter, J.; Pegram, M.; et al. Use of chemotherapy plus a monoclonal antibody against HER2 for metastatic breast cancer that overexpresses HER2. *N. Engl. J. Med.* **2001**, *344* (11), 783−792.

(5) Piccart-Gebhart, M. J.; Procter, M.; Leyland-Jones, B.; Goldhirsch, A.; Untch, M.; Smith, I.; Gianni, L.; Baselga, J.; Bell, R.; Jackisch, C.; et al. Trastuzumab after adjuvant chemotherapy in HER2-positive breast cancer. *N. Engl. J. Med.* **2005**, *353* (16), 1659−1672.

(6) Romond, E. H.; Perez, E. A.; Bryant, J.; Suman, V. J.; Geyer, C. E., Jr; Davidson, N. E.; Tan-Chiu, E.; Martino, S.; Paik, S.; Kaufman, P. A.; et al. Trastuzumab plus adjuvant chemotherapy for operable HER2-positive breast cancer. *N. Engl. J. Med.* **2005**, *353* (16), 1673−1684.

(7) Slamon, D.; Eiermann, W.; Robert, N.; Pienkowski, T.; Martin, M.; Press, M.; Mackey, J.; Glaspy, J.; Chan, A.; Pawlicki, M.; et al. Adjuvant trastuzumab in HER2-positive breast cancer. *N. Engl. J. Med.* **2011**, *365* (14), 1273−1283.

(8) Bang, Y. J.; Van Cutsem, E.; Feyereislova, A.; Chung, H. C.; Shen, L.; Sawaki, A.; Lordick, F.; Ohtsu, A.; Omuro, Y.; Satoh, T.; et al. Trastuzumab in combination with chemotherapy versus chemotherapy alone for treatment of HER2-positive advanced gastric or gastro-oesophageal junction cancer (ToGA): a phase 3, open-label, randomised controlled trial. *Lancet* **2010**, *376* (9742), 687−697.

(9) van Oers, M. H.; Van Glabbeke, M.; Giurgea, L.; Klasa, R.; Marcus, R. E.; Wolf, M.; Kimby, E.; van t Veer, M.; Vranovsky, A.; Holte, H.; et al. Rituximab maintenance treatment of relapsed/resistant follicular non-Hodgkin's lymphoma: long-term outcome of the EORTC 20981 phase III randomized intergroup study. *J. Clin. Oncol* **2010**, *28* (17), 2853−2858.

(10) Salles, G.; Seymour, J. F.; Offner, F.; López-Guillermo, A.; Belada, D.; Xerri, L.; Feugier, P.; Bouabdallah, R.; Catalano, J. V.; Brice, P.; et al. Rituximab maintenance for 2 years in patients with high tumour burden follicular lymphoma responding to rituximab plus chemotherapy (PRIMA): a phase 3, randomised controlled trial. *Lancet* **2011**, *377* (9759), 42−51.

(11) Hallek, M.; Fischer, K.; Fingerle-Rowson, G.; Fink, A. M.; Busch, R.; Mayer, J.; Hensel, M.; Hopfinger, G.; Hess, G.; von Grünhagen, U.; et al. Addition of rituximab to fludarabine and cyclophosphamide in patients with chronic lymphocytic leukaemia: a randomised, open-label, phase 3 trial. *Lancet* **2010**, *376* (9747), 1164−1174.

(12) Robak, T.; Dmoszynska, A.; Solal-Céligny, P.; Warzocha, K.; Loscertales, J.; Catalano, J.; Afanasiev, B. V.; Larratt, L.; Geisler, C. H.; Montillo, M.; et al. Rituximab plus fludarabine and cyclophosphamide prolongs progression-free survival compared with fludarabine and cyclophosphamide alone in previously treated chronic lymphocytic leukemia. *J. Clin. Oncol* **2010**, *28* (10), 1756−1765.

(13) Verma, S.; Miles, D.; Gianni, L.; Krop, I. E.; Welslau, M.; Baselga, J.; Pegram, M.; Oh, D. Y.; Dieras, V.; Guardino, E.; et al. Trastuzumab emtansine for HER2-positive advanced breast cancer. *N. Engl. J. Med.* **2012**, *367* (19), 1783−1791.

(14) Modi, S.; Saura, C.; Yamashita, T.; Park, Y. H.; Kim, S. B.; Tamura, K.; Andre, F.; Iwata, H.; Ito, Y.; Tsurutani, J.; et al. Trastuzumab Deruxtecan in Previously Treated HER2-Positive Breast Cancer. *N. Engl. J. Med.* **2020**, *382* (7), 610−621.

(15) Shitara, K.; Bang, Y. J.; Iwasa, S.; Sugimoto, N.; Ryu, M. H.; Sakai, D.; Chung, H. C.; Kawakami, H.; Yabusaki, H.; Lee, J.; et al. Trastuzumab Deruxtecan in Previously Treated HER2-Positive Gastric Cancer. *N. Engl. J. Med.* **2020**, *382* (25), 2419−2430.

(16) Witzig, T. E.; Gordon, L. I.; Cabanillas, F.; Czuczman, M. S.; Emmanouilides, C.; Joyce, R.; Pohlman, B. L.; Bartlett, N. L.; Wiseman, G. A.; Padre, N.; et al. Randomized controlled trial of yttrium-90-labeled ibritumomab tiuxetan radioimmunotherapy versus rituximab immunotherapy for patients with relapsed or refractory low-grade, follicular, or transformed B-cell non-Hodgkin's lymphoma. *J. Clin. Oncol* **2002**, *20* (10), 2453−2463.

(17) Morschhauser, F.; Radford, J.; Van Hoof, A.; Vitolo, U.; Soubeyran, P.; Tilly, H.; Huijgens, P. C.; Kolstad, A.; d'Amore, F.; Gonzalez Diaz, M.; et al. Phase III trial of consolidation therapy with yttrium-90-ibritumomab tiuxetan compared with no additional therapy after first remission in advanced follicular lymphoma. *J. Clin. Oncol* **2008**, *26* (32), 5156−5164.

(18) Rizzieri, D. Zevalin® (ibritumomab tiuxetan): After more than a decade of treatment experience, what have we learned? *Crit. Rev. Oncol. Hematol* **2016**, *105*, 5−17.

(19) Zalutsky, M. R.; Pruszynski, M. Astatine-211: production and availability. *Curr. Radiopharm.* **2011**, *4* (3), 177−185.

(20) Johnson, E. L.; Turkington, T. G.; Jaszczak, R. J.; Gilland, D. R.; Vaidyanathan, G.; Greer, K. L.; Coleman, R. E.; Zalutsky, M. R. Quantitation of ^{211}At in small volumes for evaluation of targeted radiotherapy in animal models. *Nucl. Med. Biol.* **1995**, *22* (1), 45−54.

(21) Watabe, T.; Kaneda-Nakashima, K.; Liu, Y.; Shirakami, Y.; Ooe, K.; Toyoshima, A.; Shimosegawa, E.; Fukuda, M.; Shinohara, A.; Hatazawa, J. Enhancement of ^{211}At Uptake via the Sodium Iodide

https://doi.org/10.1021/acs.molpharmaceut.2c00869
Mol. Pharmaceutics 2023, 20, 1156−1167

Symporter by the Addition of Ascorbic Acid in Targeted α-Therapy of Thyroid Cancer. *J. Nucl. Med.* **2019**, *60* (9), 1301−1307.
(22) McDevitt, M. R.; Finn, R. D.; Ma, D.; Larson, S. M.; Scheinberg, D. A. Preparation of alpha-emitting ^{213}Bi-labeled antibody constructs for clinical use. *J. Nucl. Med.* **1999**, *40* (10), 1722−1727.
(23) Pozzi, O. R.; Zalutsky, M. R. Radiopharmaceutical chemistry of targeted radiotherapeutics, part 1: effects of solvent on the degradation of radiohalogenation precursors by ^{211}At alpha-particles. *J. Nucl. Med.* **2005**, *46* (4), 700−706.
(24) Wahl, R. L.; Wissing, J.; del Rosario, R.; Zasadny, K. R. Inhibition of autoradiolysis of radiolabeled monoclonal antibodies by cryopreservation. *J. Nucl. Med.* **1990**, *31* (1), 84−89.
(25) Chakrabarti, M. C.; Le, N.; Paik, C. H.; De Graff, W. G.; Carrasquillo, J. A. Prevention of radiolysis of monoclonal antibody during labeling. *J. Nucl. Med.* **1996**, *37* (8), 1384−1388.
(26) Salako, Q. A.; O'Donnell, R. T.; DeNardo, S. J. Effects of radiolysis on yttrium-90-labeled Lym-1 antibody preparations. *J. Nucl. Med.* **1998**, *39* (4), 667−670.
(27) Ferens, J. M.; Krohn, K. A.; Beaumier, P. L.; Brown, J. P.; Hellström, I.; Hellström, K. E.; Carrasquillo, J. A.; Larson, S. M. High-level iodination of monoclonal antibody fragments for radiotherapy. *J. Nucl. Med.* **1984**, *25* (3), 367−370.
(28) Larsen, R. H.; Bruland, Ø. S. Radiolysis of radioimmunoconjugates. Reduction in antigen-binding ability by α-particle radiation. *Journal of Labelled Compounds and Radiopharmaceuticals* **1995**, *36* (10), 1009−1018.
(29) Takashima, H.; Koga, Y.; Manabe, S.; Ohnuki, K.; Tsumura, R.; Anzai, T.; Iwata, N.; Wang, Y.; Yokokita, T.; Komori, Y.; et al. Radioimmunotherapy with an ^{211}At-labeled anti-tissue factor antibody protected by sodium ascorbate. *Cancer Sci.* **2021**, *112* (5), 1975−1986.
(30) Manabe, S.; Takashima, H.; Ohnuki, K.; Koga, Y.; Tsumura, R.; Iwata, N.; Wang, Y.; Yokokita, T.; Komori, Y.; Usuda, S.; et al. Stabilization of an ^{211}At-Labeled Antibody with Sodium Ascorbate. *ACS Omega* **2021**, *6* (23), 14887−14895.
(31) Takashima, H.; Koga, Y.; Tsumura, R.; Yasunaga, M.; Tsuchiya, M.; Inoue, T.; Negishi, E.; Harada, M.; Yoshida, S.; Matsumura, Y. Reinforcement of antitumor effect of micelles containing anticancer drugs by binding of an anti-tissue factor antibody without direct cytocidal effects. *J. Controlled Release* **2020**, *323*, 138−150.
(32) Sajjad, M.; Riaz, U.; Yao, R.; Bernacki, R. J.; Abouzied, M.; Erb, D. A.; Chaudhary, N. D.; Veith, J. M.; Georg, G. I.; Nabi, H. A. Investigation of 3′-debenzoyl-3′-(3-([^{124}I]-iodobenzoyl))paclitaxel analog as a radio-tracer to study multidrug resistance in vivo. *Appl. Radiat. Isot.* **2012**, *70* (8), 1624−1631.
(33) Aneheim, E.; Gustafsson, A.; Albertsson, P.; Bäck, T.; Jensen, H.; Palm, S.; Svedhem, S.; Lindegren, S. Synthesis and Evaluation of Astatinated *N*-[2-(Maleimido)ethyl]-3-(trimethylstannyl)benzamide Immunoconjugates. *Bioconjugate Chem.* **2016**, *27* (3), 688−697.
(34) Lindmo, T.; Boven, E.; Cuttitta, F.; Fedorko, J.; Bunn, P. A., Jr Determination of the immunoreactive fraction of radiolabeled monoclonal antibodies by linear extrapolation to binding at infinite antigen excess. *J. Immunol. Methods* **1984**, *72* (1), 77−89.
(35) Coenen, H. H.; Gee, A. D.; Adam, M.; Antoni, G.; Cutler, C. S.; Fujibayashi, Y.; Jeong, J. M.; Mach, R. H.; Mindt, T. L.; Pike, V. W.; et al. Consensus nomenclature rules for radiopharmaceutical chemistry - Setting the record straight. *Nucl. Med. Biol.* **2017**, *55*, v−xi.
(36) Zalutsky, M. R.; Zhao, X. G.; Alston, K. L.; Bigner, D. High-level production of alpha-particle-emitting ^{211}At and preparation of ^{211}At-labeled antibodies for clinical use. *J. Nucl. Med.* **2001**, *42* (10), 1508−1515.
(37) Zalutsky, M. R.; Reardon, D. A.; Akabani, G.; Coleman, R. E.; Friedman, A. H.; Friedman, H. S.; McLendon, R. E.; Wong, T. Z.; Bigner, D. D. Clinical experience with alpha-particle emitting ^{211}At: treatment of recurrent brain tumor patients with ^{211}At-labeled chimeric antitenascin monoclonal antibody 81C6. *J. Nucl. Med.* **2008**, *49* (1), 30−38.
(38) Vaidyanathan, G.; Pozzi, O. R.; Choi, J.; Zhao, X. G.; Murphy, S.; Zalutsky, M. R. Labeling Monoclonal Antibody with α-emitting ^{211}At at High Activity Levels via a Tin Precursor. *Cancer Biother. Radiopharm* **2020**, *35* (7), 511−519.
(39) Hallqvist, A.; Bergmark, K.; Bäck, T.; Andersson, H.; Dahm-Kähler, P.; Johansson, M.; Lindegren, S.; Jensen, H.; Jacobsson, L.; Hultborn, R.; et al. Intraperitoneal α-Emitting Radioimmunotherapy with ^{211}At in Relapsed Ovarian Cancer: Long-Term Follow-up with Individual Absorbed Dose Estimations. *J. Nucl. Med.* **2019**, *60* (8), 1073−1079.
(40) Li, Y.; Hamlin, D. K.; Chyan, M. K.; Wong, R.; Dorman, E. F.; Emery, R. C.; Woodle, D. R.; Manger, R. L.; Nartea, M.; Kenoyer, A. L.; et al. cGMP production of astatine-211-labeled anti-CD45 antibodies for use in allogeneic hematopoietic cell transplantation for treatment of advanced hematopoietic malignancies. *PLoS One* **2018**, *13* (10), No. e0205135.
(41) Hotte, C. E.; Ice, R. D.; Flynn, G. L. Radiolysis of ^{131}I-O-iodohippurate: A kinetic study. *Journal of Labelled Compounds and Radiopharmaceuticals* **1980**, *17* (5), 715−725.
(42) COENEN, H. H.; MOERLEIN, S. M.; STÖCKLIN, G. No-Carrier-Added Radiohalogenation Methods with Heavy Halogens. *Radiochim. Acta* **1983**, *34* (1−2), 47−68.
(43) Ayed, T.; Pilmé, J.; Tézé, D.; Bassal, F.; Barbet, J.; Chérel, M.; Champion, J.; Maurice, R.; Montavon, G.; Galland, N. ^{211}At-labeled agents for alpha-immunotherapy: On the *in vivo* stability of astatine-agent bonds. *Eur. J. Med. Chem.* **2016**, *116*, 156−164.
(44) Dekempeneer, Y.; Bäck, T.; Aneheim, E.; Jensen, H.; Puttemans, J.; Xavier, C.; Keyaerts, M.; Palm, S.; Albertsson, P.; Lahoutte, T.; et al. Labeling of Anti-HER2 Nanobodies with Astatine-211: Optimization and the Effect of Different Coupling Reagents on Their in Vivo Behavior. *Mol. Pharmaceutics* **2019**, *16* (8), 3524−3533.
(45) Teze, D.; Sergentu, D. C.; Kalichuk, V.; Barbet, J.; Deniaud, D.; Galland, N.; Maurice, R.; Montavon, G. Targeted radionuclide therapy with astatine-211: Oxidative dehalogenation of astatobenzoate conjugates. *Sci. Rep.* **2017**, *7* (1), 2579.
(46) Larsen, R. H.; Slade, S.; Zalutsky, M. R. Blocking [^{211}At]-astatide accumulation in normal tissues: preliminary evaluation of seven potential compounds. *Nucl. Med. Biol.* **1998**, *25* (4), 351−357.
(47) Liu, Y.; Watabe, T.; Kaneda-Nakashima, K.; Ooe, K.; Shirakami, Y.; Toyoshima, A.; Shimosegawa, E.; Nakano, T.; Shinohara, A.; Hatazawa, J. Preclinical Evaluation of Radiation-Induced Toxicity in Targeted Alpha Therapy Using [^{211}At] NaAt in Mice: A Revisit. *Transl. Oncol* **2020**, *13* (4), 100757.
(48) Spetz, J.; Rudqvist, N.; Forssell-Aronsson, E. Biodistribution and dosimetry of free ^{211}At, ^{125}I- and ^{131}I- in rats. *Cancer Biother. Radiopharm* **2013**, *28* (9), 657−664.
(49) Lub-de Hooge, M. N.; Kosterink, J. G.; Perik, P. J.; Nijnuis, H.; Tran, L.; Bart, J.; Suurmeijer, A. J.; de Jong, S.; Jager, P. L.; de Vries, E. G. Preclinical characterisation of ^{111}In-DTPA-trastuzumab. *Br. J. Pharmacol.* **2004**, *143* (1), 99−106.
(50) Kristensen, L. K.; Christensen, C.; Jensen, M. M.; Agnew, B. J.; Schjöth-Frydendahl, C.; Kjaer, A.; Nielsen, C. H. Site-specifically labeled ^{89}Zr-DFO-trastuzumab improves immuno-reactivity and tumor uptake for immuno-PET in a subcutaneous HER2-positive xenograft mouse model. *Theranostics* **2019**, *9* (15), 4409−4420.
(51) Yoon, J. T.; Longtine, M. S.; Marquez-Nostra, B. V.; Wahl, R. L. Evaluation of Next-Generation Anti-CD20 Antibodies Labeled with ^{89}Zr in Human Lymphoma Xenografts. *J. Nucl. Med.* **2018**, *59* (8), 1219−1224.
(52) Howell, G. L.; Van Middlesworth, L. Gastric iodide and chloride clearances in dogs. *Proc. Soc. Exp. Biol. Med.* **1956**, *93* (3), 602−605.
(53) Logothetopoulos, J. H.; Myant, N. B. Concentration of radio-iodide and ^{35}S-labelled thiocyanate by the stomach of the hamster. *J. Physiol* **1956**, *133* (1), 213−219.

https://doi.org/10.1021/acs.molpharmaceut.2c00869
Mol. Pharmaceutics 2023, 20, 1156−1167